INTERNATIONAL JOURNAL OF ENERGY RESEARCH
Int. J. Energy Res. 2011; **35**:1056–1074
Published online 17 March 2011 in Wiley Online Library (wileyonlinelibrary.com). DOI: 10.1002/er.1835

Correlation model of mixed ionic–electronic conductivity in solid oxide lattices in the presence of point and line defects for solid oxides fuel cells

Sebastiano Tosto*,†

ENEA Casaccia, via Anguillarese 301, 00123 Roma, Italy

SUMMARY

This paper concerns a 3D mathematical model about the mixed ionic–electronic conductivity in solid oxides in the presence of point and line lattice defects. It is known that the presence of vacancies increases the ionic conductivity; moreover, there is experimental evidence that samples with large compression strains exhibit higher conductivity, which supports the idea that the ion mobility inside the solid oxide is enhanced by a high density of dislocations. The present model aims to show that the diffusion rate of ions is enhanced by the lattice stress field of dislocations properly oriented with respect to the electric potential gradient. Simple considerations quantify the interaction of the ions with the stress field and demonstrate that the presence of dislocations in the crystal lattice causes a drift force additional to that due to the concentration and electric potential gradients; thus, explaining the increase of conductivity experimentally evidenced. Although the model concerns for simplicity a homogeneous and isotropic single crystal of solid oxide, the information provided is of direct interest also for the case of polycrystalline solid oxides with grain boundaries. Copyright © 2011 John Wiley & Sons, Ltd.

KEY WORDS

solid oxide fuel cell; model; ionic conduction

Correspondence

*Sebastiano Tosto, ENEA Casaccia, via Anguillarese 301, 00123 Roma, Italy.
†E-mail: sebastiano.tosto@enea.it;stosto@inwind.it

Received 20 December 2010; Revised 1 February 2011; Accepted 2 February 2011

1. INTRODUCTION

One of the main challenges of the SOFC technology is to design a solid oxide electrolyte with ion conductivity of the order of $0.1\,S\,cm^{-1}$ at low-intermediate temperatures in the range of 300–600°C. Unfortunately, conductivities of this order of magnitude are today achieved at higher temperatures only; e.g. about 1000°C is necessary for yttrium-stabilized zirconia, whereas doped ceria electrolytes have comparable conductivity at temperatures of the order of 800°C. Thin film electrolytes allow to reduce further the working temperature down to about 700°C; however, with serious problems of microstructural degradation at long service times. Moreover, innovative nano-scale-structured materials prospect the chance of acceptable conductivity at even lower temperatures that encourage new market perspectives for the SOFC commercialization. In this scenario of multidisciplinary research, the contribution of theoretical modelling on the mechanisms of ion transport in solid oxides to rationalize the experimental activity appears especially useful. The computer modelling aims in general to understand the basic mechanisms that control the performances of the fuel cells. A great variety of models is reported in the literature on catalysis [1], chemisorption [2], mechanisms of oxygen reduction [3], porosity of composite electrodes [4] and ion transport in nanocrystalline materials [5]. An outline of multi-scale modelling as a predictive tool for various engineering aspects of fuels cells is reported in [6]. Moreover, electrochemical impedance techniques are also simulated by means of atomic scale computer models that exploit Monte Carlo probabilistic calculations of jumping events based on known reaction rates [7]. Usually in atomic scale models the number of atoms used for the simulation is upper limited by the computing time; the functional density theory partially removes the mathematical difficulty arising from the many body potential term, introducing the particle density in the corresponding ground quantum state wave function. Hence, the observables, in particular

the ground state energy, are a functional of particle density that fulfils the condition of minimizing the total energy. Drastic approximations are, however, necessary to carry out these kinds of calculations. As a valid alternative, the macro-scale models exploit the known transport equations in the presence of an electric potential gradient to provide useful information in the cases where very large numbers of atoms/ions are necessarily involved. This kind of approach is introduced in the present paper to explain why a high density of dislocations properly oriented with respect to the potential gradient enhances the ionic conductivity of solid oxides; the experimental evidence that samples with large compression strains exhibit higher conductivity [8] indeed supports the idea that the local modification of the stress field around a dislocation is a leading mechanism responsible for the enhanced conductivity. The present model shows that the stress field induced by the presence of edge and screw dislocations in the lattice of solid oxides affects the diffusion rate of charge carriers. The model assumes a homogeneous and isotropic solid oxide single crystal at constant equilibrium temperature T. For simplicity, phase transitions are excluded at the temperature considered.

2. PHYSICAL BACKGROUND OF THE MODEL

Consider first a single crystal lattice of non-porous and defect-free solid oxide at time t and temperature T. This preliminary assumption, initially introduced having in mind the bulk region of one ideal grain only, will then be gradually extended to the more complex and realistic case of a polycrystalline solid oxide and implemented to account for the presence of point and line lattice defects too. Starting with the simplest case, the 3D mass drift/diffusion equation under electrical and chemical potentials reads

$$\begin{aligned} &\mathbf{J}_i^{\text{mass}} = -D_i\nabla c_i - \frac{\sigma_i}{z_i e}\nabla\phi, \quad D_i = D_i(c_i, T), \\ &c_i = c_i(x, y, z, t), \quad \sigma_i = \sigma_i(x, y, z, t), \\ &\phi = \phi(x, y, z, t) \end{aligned} \tag{1}$$

where D_i is the diffusion coefficient of the ith species, c_i the concentration, σ_i the conductivity, ϕ the electrical potential and $z_i e$ the charge carried by the species. D_i is assumed not to depend on the orientation of the crystal planes in isotropic solid oxides; regarding it as an average value avoids introducing it as a tensor. In addition, the following considerations should more properly deal with activities rather than concentrations of charge carriers present in the lattice; yet the mathematical features of the model remain basically the same irrespective of either way to regard c_i. Let the concentrations be expressed as mol per unit volume; then the fluxes $\mathbf{J}_i^{\text{mass}}$ and $\mathbf{J}_i^{\text{charge}}$ of mass and charge of the ith charge carrier, having physical dimensions of number of moles and charges per unit surface and time, are linked by $\mathbf{J}_i^{\text{charge}} = z_i e\mathbf{J}_i^{\text{mass}}$. In Equation (1) $\mathbf{J}_i^{\text{mass}}$ is a linear combination of diffusion and ohmic terms $\mathbf{J}_i^{\text{diff}} = -D_i\nabla c_i$ and $\mathbf{J}_i^{\text{ohm}} = -\sigma_i\nabla\phi/z_i e$ describing the charge fluxes under effect of concentration and electric potential gradients; here $\sigma_i = (z_i e)^2 c_i D_i/kT$. According to the scheme reported in [9] let us introduce also the mass continuity condition, i.e. there are neither sources nor sinks of carriers in the electrolyte, and the Poisson electric potential equation. As $z_i e c_i$ has physical meaning of charge carried by the current number of moles per unit volume, it is possible to write

$$\begin{aligned} &\nabla\cdot\mathbf{J}_i^{\text{mass}} + \frac{\partial c_i}{\partial t} = 0, \\ &-(\varepsilon_r\varepsilon_0)\nabla^2\phi = \sum_j e z_j (c_j - c_j^0), \quad c_i^0 = c_i(t=0) \end{aligned} \tag{2}$$

where ε_0 is the permittivity of vacuum and ε_r the relative dielectric constant of the solid oxide. The second equation yields the electric potential as a function of the total charge density; the notation aims to avoid possible confusion between the index i that labels a particular ion and the summation index j over all the ions. The constants c_i^0 introduce the initial equilibrium concentrations of ions uniformly distributed in the crystal lattice, whereas $ez_i c_i^0$ represent the respective charge per unit volume around the point of the solid oxide where the ith ion is initially located; similarly, $ez_i c_i$ represents the charge density around the point where c_i is defined. Thus, by definition $\sum_j z_j e c_j^0 = 0$, because of the initial electro-neutrality of the oxide crystal before the change of ion concentration due to the electric potential-driven charge flow; this assumption ensures the boundary condition $\phi = \text{const} = 0$ at $t = 0$ required for the potential, in general defined as an arbitrary constant apart. The equation describing the total charge flux that completes the system of Equations (1) and (2) is

$$\mathbf{J}_{\text{tot}}^{\text{charge}} = \sum_j \mathbf{J}_j^{\text{charge}} - \frac{\nabla\phi}{kT}\sum_j (ez_j)^2 c_j D_j$$

This equation includes the displacement flux due to the effect of a time-varying electric field, for instance that superimposed during electrode impedance measurements. This result is immediately obtained multiplying both sides of the first equation in Equation (1) by $z_i e$ and summing up to all ions; the first addend is the concentration gradient-driven flux, the second is the electric potential-driven flux that vanishes if ϕ is constant or null. The literature models report that under proper simplifying assumptions, e.g. 1D approach, these equations are solved in order to introduce an applied time-varying electrical field and then to simulate the flow of charges as in the experimental conditions of electrode impedance

technique, e.g. [9]. In this case, the Nernst–Einstein equation is appropriately exploited to express D_i as a function of σ_i and solve Equation (1) with respect to quantities determinable by experimental electrochemical measurements. Having, however, relevant theoretical interest, a different approach aimed to correlate directly ionic conductivity and microstructure of the solid oxide. For this purpose, it is more convenient to replace D_i instead of σ_i; hence, Equation (1) becomes

$$\mathbf{J}_i^{\text{mass}} = -D_i\left(\boldsymbol{\nabla} c_i + \alpha_i \frac{z_i e c_i}{kT}\boldsymbol{\nabla}\phi\right)$$

The electrical term also introduces a correlation coefficient α_i relating self-diffusion and ionic conduction. Although this coefficient typically varies between 0.5 and 1 and is usually ignored [10], it is retained here to enhance the completeness of the present model. Hence,

$$\boldsymbol{\nabla}\cdot\left[D_i\left(\boldsymbol{\nabla} c_i + \alpha_i \frac{z_i e c_i}{kT}\boldsymbol{\nabla}\phi\right)\right] - \frac{\partial c_i}{\partial t} = 0 \qquad (3)$$

Hence, Equation (3) describes the ion transport of the ith element in a solid oxide electrolyte as a function of its microstructure through D_i explicitly retained. It is known that the microstructure determines the value of the diffusion coefficient, a complex quantity dependent in general on the concentration through the activity coefficient β_i of the diffusing species. The Darken equation expresses the transport rate as a function of the chemical potential gradient μ, more appropriately than via the concentration gradient; it is easy to show that [11]

$$D_i = L_i\frac{\partial \mu_i}{\partial c_i} = kT\frac{L_i}{c_i}\left(1+\frac{\partial \ln \beta_i}{\partial \ln c_i}\right),$$
$$\mu_i = kT\ln(c_i\beta_i)$$

where μ_i is the chemical potential and L_i the product of concentration and average mobility B_i of the ith ion; the latter is defined as the ratio between drift velocity and applied force, then $B_i = L_i/c_i$. Since the product kTL_i/c_i has physical meaning of diffusion coefficient according to the Einstein equation $D_i = B_i kT$, a useful form of diffusion coefficient is

$$D_i = \left(1+\frac{\partial \ln \beta_i}{\partial \ln c_i}\right)D_{oi}\exp(-E_{ai}/kT),$$
$$D_{oi} = D_{oi}(v_i) \qquad (4)$$

This expression contains three factors: the first related to the chemical potential gradient via β_i and c_i that reduces to 1 if the activity coefficient is constant, the second related to the jump frequency v_i, the third to the jump activation energy E_{ai}. Equation (4) shows the basic ingredients that link at any temperature the diffusion coefficient to the microstructure in the presence of lattice point defects under electric and concentration gradients. It is useful to highlight how D_i of Equation (2) is related to that concerned here. Consider first c_i^0 in a defect-free ideal perfect crystal; Equation (4) yields then a value D_i^{0id}. In the real case of a crystal with vacancies, $D_i^0 > D_i^{0id}$ even though assuming the same c_i^0 as before because now $v_i > v_i^{id}$ and $E_{ai} < E_{ai}^{id}$. Therefore, D_i^0 is the common diffusion coefficient measurable experimentally for each ion in a dislocation-free solid oxide with a given chemical composition. If $c_i > c_i^0$ one expects that the higher amount of ions flowing in the crystal increases the local lattice strain and then the related number of point defects, so that $D_i > D_i^0$; this is typically the case where ions are generated at the electrodes of a fuel cell and cross the solid oxide electrolyte under an electric potential. Note that a vacancy is regarded in general as a particle occupying a definite site in the solid oxide electrolyte; as emphasized by the Kröger–Vink notation, a local excess of p-type or n-type charge with respect to the neutral lattice can be assigned to it even if no current circulates in the electrolyte. A typical case particularly important, the oxygen vacancy concentration in a solid oxide with homovalent or aliovalent dopants, stimulates defining for the sake of generality one among the initial ith concentrations, say $c_{i\pm}^0$, as amount of localized charge originally existing in the lattice by consequence of its point defect structural features [12]. Then, when the cell is working and the ion current strains dynamically the lattice along its path, one expects also a current of charges driven by the cloud of newly formed vacancies; according to this idea $c_{i\pm}^0$ increases to $c_{i\pm}$ whereas the model concerns in fact flows of ions coupled with flows of vacancy-driven electric charges, both crossing the electrolyte by effect of the electrochemical potential. For brevity only, the whole flow of charge carriers will be referred to in the following as ion flow. Without considering the lattice line defects, therefore, D_i of Equation (2) is a complicated function $D_i(T, \beta_i, c_i, E_{ai}, v_i, \phi, x, y, z, t)$ of the microstructure and working conditions of the cell, e.g. its operating temperature. Note that here we have considered the lattice strain due to the increased concentration of ions in the crystal only, neglecting however that due in principle also to the presence of the vacancies themselves; owing to the local character of lattice perturbation induced by these latter, D_i is adequately described by appropriate values of E_{ai} and v_i. In the presence of dislocations, even though this is no longer true; long-range stress action at distances much higher than the crystal spacing is to be expected. This fact justifies the efforts reported in the literature to modify the ionic conductivity of solid oxides through heat treatments aimed to control the carefully amount and nature of lattice defects. An interesting example is that related to the concept of ion highway [13]: the ionic conductivity of thin film electrolytes (50–290 nm thick) of YSZ is significantly increased by dislocations structured in order to allow high mobility of O^{-2} ions via a proper annealing treatment enabling elimination of point defects and growth of dislocations [14]. Let us account, for this experimental situation introducing first into Equation (3), the stress field of one edge dislocation only; the

preliminary simulation of possible fast transport in the crystal of solid oxide can then be generalized to account for an arbitrary number and orientation of dislocations. Some basic concepts of materials physics can reasonably be exploited for this purpose; the mechanisms responsible for the lattice stress–displacements are not specific on a particular class of materials only, but rest on general principles of the elastic theory of solids. It is known that the shear stress component σ_{xy} of an edge dislocation on the plane at distance y above the slip plane is [15]

$$\sigma_{xy} = \frac{Gb}{2\pi(1-v)}\frac{\sin(4\theta)}{4y}$$

where G is the shear modulus, $b = |\mathbf{b}|$ with $\mathbf{b}$ the Burgers vector, θ the lattice distortion angle induced by the dislocation on the neighbour crystal planes and v the Poisson modulus. The force per unit length of edge dislocation related to the shear stress is $F = b\sigma_{xy}$. This result, valid to calculate the force acting on another dislocation, is exploited here to estimate the force to which an ion interacting with the stress field of the dislocation is subjected. If λ is the line length of the dislocation, then

$$\mathbf{F} = \frac{Gb^2\lambda}{2\pi(1-v)}\frac{\sin(4\theta)}{4y}\mathbf{b}_{\text{un}}, \quad \mathbf{b} = b\mathbf{b}_{\text{un}}$$

where $\mathbf{b}_{\text{un}}$ is a unit vector oriented like the Burgers vector. The force $\mathbf{F}$, linearly decreasing far from the slip plane, has an interaction range typically of the order of 10^{-4} cm in metals [16]; it is reasonable to expect that within this range it perturbs the motion of the ion and then modifies its drift velocity, as in effect the lattice defects interrupt the regular stack of crystal planes and thus somehow perturb the flux of charge carriers running through the lattice. This means regarding $\mathbf{F}$ as a generalized thermodynamic force present in a real crystal of solid oxide, whose effect is to modify the ion drift velocity allowed in a perfect lattice by a feature component $\mathbf{v}_i^d$. Hence, once having justified from a micro-scale point of view the idea that the lattice defects affect the ion flow, the results just obtained allow inserting also this force in the present macro-scale model. Recall in this respect the basic assumption of diffusion theory $\mathbf{J}^{\text{mass}} = -Bc\nabla\mu$; i.e. the mass flow $\mathbf{J}^{\text{mass}}$ is related to the gradient of chemical potential μ, which in turn introduces the known concept of thermodynamic force through the mobility coefficient B [11]. It is also known that the force $\mathbf{F}_\mu = -\nabla\mu$ introduces the diffusion coefficient $D_\mu = kTL/c$ taking into account the concentration c of the diffusing species [11]; it is easy to show that D_μ is related to the Darken equation written as $D/D_\mu = 1+\partial\log(\beta)/\partial\log(c)$ so that, owing to Equation (4), D_μ is also linked to the jump activation energy and frequency. It is therefore reasonable to assume that analogous reasoning holds also for a charge carrier flowing in the perturbing field of defects, so that it is possible to write for the ith ion

$$D_i^d = kTL_i/c_i, \qquad \mathbf{v}_i^d = B_i\mathbf{F}_i^d, \qquad \mathbf{J}_i^d = c_i\mathbf{v}_i^d$$

The dislocation induced mass flow $\mathbf{J}_i^d$ is then

$$\mathbf{J}_i^d = c_i\mathbf{F}_i^d D_i^d/kT$$

This result could be more directly inferred from the definition of mass flux $\mathbf{J}_i^d$, replacing $\mathbf{v}_i^d$ via the Nernst–Einstein equation that links $\mathbf{v}_i^d = B_i\mathbf{F}$ and $D_i^d = kTB_i$ to describe how the dislocation affects the ion transport; this gives indeed $\mathbf{J}_i^d = c_i\mathbf{F}D_i^d/kT$. Let us return now to Equation (3) that for $\phi = 0$ it is the well-known diffusion equation in a perfect lattice or in a lattice with defects depending on how D_i is defined according to Equation (4); for $\phi \neq 0$ this equation contains an additional term that accounts for the applied electric potential and turns into the sought form including the drift effect during the operating conditions of an electrolyte in a fuel cell. Note that the local $\mathbf{J}_i^d$ is additive with respect to $\mathbf{J}_i^{\text{mass}}$ of Equation (1) in the unperturbed lattice far from the dislocation stress field; moreover, the diffusion coefficient is uniquely defined in a given experimental situation, where $\mathbf{J}_i^{\text{mass}}$ describes the total mass flux including the concentration gradient and electric drift contributions of the first equation (1) plus the lattice stress contribution $\mathbf{J}_i^d$ oriented with the Burgers vector $\mathbf{b}$. Hence, it is possible to omit the superscript and write simply D_i even in the presence of the dislocation: in fact $D_i = D_i(x,y,z,t)$ of each ion includes in principle the local deviation of its value with respect to that of the unperturbed lattice. The same holds of course also for c_i; although formerly introduced in the equations of a perfect solid oxide lattice, from now on they must be intended as concentrations pertinent to a real lattice in the presence of an applied potential. Since Equation (1) have introduced the dependence of D_i on the local coordinates through c_i, it follows that concentration profile and stress field of the dislocation are in effect correlated. In conclusion, $\mathbf{J}_i^{\text{mass}}$ including all of the contributions just mentioned is given by

$$\mathbf{J}_i^{\text{mass}} = -D_i\left(\nabla c_i + \alpha_i\frac{z_i e c_i}{kT}\nabla\phi - \frac{c_i\mathbf{F}}{kT}\right) \tag{5}$$

so that Equation (3) reads

$$\nabla\cdot\left[D_i\left(\nabla c_i + \alpha_i\frac{z_i e c_i}{kT}\nabla\phi - \frac{c_i\mathbf{F}}{kT}\right)\right] - \frac{\partial c_i}{\partial t} = 0 \tag{6}$$

The solution of this equation provides one with the necessary information about how the charge carriers move in the presence of electric field, stress field of dislocations and lattice vacancies through $\nabla\phi$, $\mathbf{F}$ and D_i. For instance, splitting this vector equation into its corresponding x, y, z scalar equations identifies the most favourable dislocation orientation that optimizes the ion drift velocity in agreement with the given $\nabla\phi$; thus, revealing how the respective components of $\mathbf{b}$

affect c_i. Equation (5) shows that the electric and stress fields additional to the diffusive gradient term have analogous form, since $\mathbf{F}$ can be certainly expressed as the gradient of a proper scalar potential; this is not surprising since both have been introduced through the Nernst–Einstein equation not dependent on the specific nature of the driving force that defines the mobility. This result suggests therefore the existence of an effective field drift force

$$\mathbf{F}_i^{el,d} = \alpha_i z_i e \boldsymbol{\nabla}\phi - \mathbf{F} \tag{7}$$

At this point, even without solving explicitly Equation (6) together with Equations (2) and (4), some simple considerations are evident in principle. The dislocation stress field can cooperate with or oppose the electric potential gradient in controlling the dynamics of the charge carriers in the crystal depending on how the gradient is oriented with respect to the Burgers vector. Intuitive energy considerations suggest that the lattice compression due to the dislocation creates preferential ion drift directions: for instance, ion jumps across the extra plane of an edge dislocation plane are hampered, whereas they should instead be favoured jumps parallel to the extra plane. The lattice dynamics of the dislocations is well known in physical metallurgy and controls important phenomena like precipitation hardening or work hardening of alloys. These phenomena are also of present interest: for the same reason a potential energy barrier U such that $\mathrm{d}U/\mathrm{d}\mathbf{r} = -\mathbf{F}$ makes less efficient or more efficient the coexisting mechanism of jump driven ion drift depending on its vector sum with the electric potential gradient. Hence, the output of a simulation model should confirm that the presence of dislocation lines oriented in order to confine the ion drift along the electric gradient enhances the conductivity with respect to any random walk stimulated by vacancy-driven jumps only. Moreover, an additional ion channelling effect might also be expected along the lower boundary of an edge dislocation because the cell parameter just below the extra-plane is stretched with respect to that of the perfect lattice; also this effect could account for preferential channelling conditions that feature the concept itself of ion highway. Computing and numerically substantiating these effects should confirm the intuitive considerations so far shortly sketched, while providing a better understanding of the ion dynamics. From a macroscopic point of view, however, the local details on the actual motion of the ions are skipped, being instead relevant the fact that any microstructural change increasing the local values of diffusivity entails in principle enhanced values of conductivity in agreement with $\sigma_i = (z_i e)^2 c_i D_i/kT$. The approach of the present paper avoids, therefore, describing at the micro-scale level the ion transport mechanisms in the solid oxide that determine the values of D_i, which are thus regarded as input data of the model and specify the kind of solid oxide. The model focuses instead on the correlation between the various quantities that affect the values of the various D_i; it is interesting in this respect the fact that the lower the temperature, the more any given increase of D_i tends to enhance σ_i; thus, confirming the importance of the diffusivity and related microstructure of the solid oxide to decrease the operating temperature of the cell. It is eventually worth noticing that even the presence of several dislocations is in principle easily taken into account, in particular, if the force $b\sigma_{xy}$ exerted by a unit dislocation length on a similar one can be neglected; it could be the case of an annealed solid oxide lattice. If so, it is enough to replace $\mathbf{F}$ in Equation (6) with an averaged sum of terms $\sum_n \mathbf{F}_n$ extended to the actual number of dislocations with respective Burgers vector $\mathbf{b}_n$; the effective force then reads

$$\mathbf{F}_i^{el,d} = \alpha_i z_i e \boldsymbol{\nabla}\phi - \left\langle \sum_n \mathbf{F}_n \right\rangle$$

In this way, the solution of the system of 3D differential equations is certainly much more difficult from the mathematical point of view, yet certainly more realistic. Nonetheless simple considerations help to infer interesting information in principle on the effect of the stress field of any number and orientation of dislocations. In the following T will be assumed constant throughout.

3. THE MODEL

For simplicity, let us regard $\mathbf{F}$ from now on as the resultant stress field induced by many point and line lattice defects of the solid oxide crystal, i.e. implicitly assuming that the considerations concerning one dislocation only still have statistical meaning even in the presence of several dislocations. Consider preliminarily $\phi = \mathbf{0}$ in Equation (6) and the particular case of plain diffusion of the ith species, the position $c_i\mathbf{F}/kT = a_i\boldsymbol{\nabla}c_i$ yields $\boldsymbol{\nabla}\cdot[(1-a_i)D_i\boldsymbol{\nabla}c_i] - \partial c_i/\partial t = 0$, being a_i dimensionless proportionality constants. This result can still be regarded as a diffusion equation where D_i is replaced by an effective value $(1-a_i)D_i$, so that

$$\begin{gathered}\phi = \mathbf{0}, \quad \mathbf{F} = a_i\boldsymbol{\nabla}\mu_i, \quad \boldsymbol{\nabla}\cdot[D_i^*\boldsymbol{\nabla}c_i] - \partial c_i/\partial t = 0, \\ D_i^* = (1-a_i)D_i, \quad \mu_i = kT\log(c_i/c_i^0)\end{gathered} \tag{8}$$

The proposed definition of $\mathbf{F}$ leads to a reasonable result: the force exerted by the stress field of the dislocation on the ith species is proportional to the gradient of a scalar potential, i.e. the chemical potential μ_i of the ith ion due to its change of concentration in the solid oxide from the initial equilibrium value c_i^0 to the current value c_i. Hence, in the presence of dislocations an effective diffusion coefficient D_i^* is defined as a consequence of this stress field, whereas the constants a_i that link the various μ_i to $\mathbf{F}$ control the diffusion behaviour of the respective ions

in the solid oxide. Let us now examine the problem more in general and rigorously, to show that a similar result still holds even in the presence of the electric potential term. Starting again from Equation (6), let us exploit the following considerations to infer the possible form of $\mathbf{F}$: (i) the effect of a force field around a dislocation on the ion of mass m_i travelling with local drift velocity $\mathbf{v}_i$ is obviously to change its current velocity, i.e. $m_i\dot{\mathbf{v}}_i$; (ii) the presence of a dislocation modifies the local concentration of the ith species (recall for instance the Cottrel atmospheres surrounding the dislocations [17]) so that one expects a link between force and local concentration gradient, i.e. $c_i\mathbf{F}/kT \propto \boldsymbol{\nabla}c_i$ as done in Equation (8); (iii) the modified concentration of the ith charged species around the dislocation certainly affects the local electric potential as well; hence, one also expects that electric potential and $\mathbf{F} = \mathbf{F}(\phi)$ are linked by a proper function defined by the former. In conclusion, these positions suggest

$$\frac{c_i\mathbf{F}}{kT} = a_i\boldsymbol{\nabla}c_i + \Gamma_i + \frac{m_i c_i\dot{\mathbf{v}}_i}{kT}, \quad \boldsymbol{\Gamma}_i = \boldsymbol{\Gamma}_i(c_i), \quad \mathbf{v}_i = \mathbf{v}_i(c_i) \tag{9}$$

where the vectors $\boldsymbol{\Gamma}_i$ are the sought functions that link the various charge concentrations around the dislocation to the local electric potential. Inserting this expression of the force into Equation (6), one finds

$$\boldsymbol{\nabla}\cdot\left[D_i\left((1-a_i)\boldsymbol{\nabla}c_i + \alpha_i\frac{z_i e c_i}{kT}\boldsymbol{\nabla}\phi - \boldsymbol{\Gamma}_i\right) + \frac{m_i\mathbf{v}_i}{kT}\frac{\partial(D_i c_i)}{\partial t}\right] = \frac{\partial C_i}{\partial t}, \quad C_i = c_i + \frac{m_i\boldsymbol{\nabla}\cdot(c_i D_i\mathbf{v}_i)}{kT} \tag{10}$$

The second equation (10) introduces new concentrations C_i related to the respective c_i through the divergence of the vector $c_i D_i\mathbf{v}_i$ representing an energy per unit surface. This result strongly suggests that this vector is solenoidal, i.e. its divergence is null so that actually $C_i \equiv c_i$; this means that each charged species moves as an incompressible fluid whose net flow across any closed surface within the electrolyte is null, in agreement with the fact that the early diffusion equation (6) requires neither sink nor sources of charge carriers within the solid oxide. Before proving this conclusion, the notation C_i is still used. Let us rewrite now the first equation (10) exploiting the following positions

$$\boldsymbol{\nabla}c_i + \frac{z_i e c_i}{kT}\boldsymbol{\nabla}\phi = \frac{z_i e c_i}{kT}\boldsymbol{\nabla}\mu_i^{\mathrm{tot}}, \quad \mu_i^{\mathrm{tot}} = \frac{\mu_i}{z_i e} + \phi, \quad a_i = 1 - \alpha_i$$

The fact of having found through the position at left-hand side the term μ_i^{tot} including the electrical equivalent $\mu_i/z_i e$ of the chemical potential, formerly introduced in [9], supports the present choice to define the coefficients a_i that characterize $\mathbf{F}$. With these positions Equation (6) reads

$$\boldsymbol{\nabla}\cdot\left[\frac{m_i\mathbf{v}_i}{kT}\frac{\partial(D_i c_i)}{\partial t} - D_i\boldsymbol{\Gamma}_i + \frac{D_i z_i e c_i}{kT}\alpha_i\boldsymbol{\nabla}\left(\phi + \frac{\mu_i}{z_i e}\right)\right] = \frac{\partial C_i}{\partial t} \tag{11}$$

Introduce now the functions $\boldsymbol{\Gamma}_i$ as follows

$$-\boldsymbol{\Gamma}_i + \frac{z_i e c_i}{kT}\alpha_i\boldsymbol{\nabla}\left(\phi + \frac{\mu_i}{z_i e}\right) = \frac{z_i e\phi_{oi}}{kT}\alpha_i\boldsymbol{\nabla}c_i, \quad \phi_{oi} = \phi_{oi}(c_i) \tag{12}$$

where the functions ϕ_{oi} have physical dimension of electric potential; actually this position does not yet define $\boldsymbol{\Gamma}_i$, which are merely expressed through new functions ϕ_{oi}. Hence, Equation (10) reads

$$\boldsymbol{\nabla}\cdot\left[\frac{m_i\mathbf{v}_i}{kT}\frac{\partial(D_i c_i)}{\partial t} + \frac{z_i e\phi_{oi}}{kT}\alpha_i D_i\boldsymbol{\nabla}c_i\right] = \frac{\partial C_i}{\partial t} \tag{13}$$

This yields eventually, with the help of the previous definition of C_i in Equation (10),

$$\boldsymbol{\nabla}\cdot[(D_i^* + D_i^{\S})\boldsymbol{\nabla}C_i] = \frac{\partial C_i}{\partial t}, \quad D_i^* = \frac{z_i e\phi_{oi}}{kT}\alpha_i D_i, \quad \frac{m_i\mathbf{v}_i}{kT}\frac{\partial(c_i D_i)}{\partial t} = D_i^*\boldsymbol{\nabla}(C_i - c_i) + D_i^{\S}\nabla C_i \tag{14}$$

As expected, the first equation (14) shows that the initial diffusion equation (6) is modified by Equation (9) as in Equation (8): the plain diffusion coefficient D_i of the ith ion in the solid oxide introduced in Equation (4) is replaced by the effective value $D_i^{\mathrm{eff}} = D_i^* + D_i^{\S}$ that takes into account the total driving force acting on the ith ion in the presence of concentration and electric potential gradients. The physical meaning of $D_i^{\S}$ and D_i^{eff} is highlighted considering the third Equation (14); the scalar product of both sides of this equation by the operator $\boldsymbol{\nabla}$ yields with the help of Equation (10),

$$-\frac{\partial c_i}{\partial t} - \frac{m_i}{kT}\boldsymbol{\nabla}\cdot\left[c_i D_i\frac{\partial\mathbf{v}_i}{\partial t}\right] = -\boldsymbol{\nabla}\cdot[D_i^*\boldsymbol{\nabla}c_i] \tag{15}$$

This result suggests putting

$$\frac{m_i}{kT}c_i D_i\frac{\partial\mathbf{v}_i}{\partial t} = -D_i^{\S}\boldsymbol{\nabla}c_i + \mathbf{B}_i, \quad \mathbf{B}_i = \mathbf{B}_i(x, y, z, t) \tag{16}$$

In principle this position agrees with the idea that the vector $c_i D_i\partial\mathbf{v}_i/\partial t$ has physical dimension of energy flowing along the direction of $\partial\mathbf{v}_i/\partial t$; being kT/m_i an energy per unit mass, the ratio on the left-hand side is an energy flow normalized to energy per unit mass, namely it is a mass flow. This justifies the presence of the diffusion coefficient on the right-hand side; the vector term accounts for the fact that the flow on the left-hand side is not necessarily diffusive only. Thanks to the fact that in particular the diffusion coefficient is put just equal to $D_i^{\S}$ of the third Equation (14),

Equation (15) turns into

$$\frac{\partial c_i}{\partial t}=\nabla\cdot[(D_i^{*}+D_i^{\S})\nabla c_i],\quad D_{c_i}^{\mathrm{eff}}=D_i^{*}+D_i^{\S},$$
$$\nabla\cdot\mathbf{B}_i=0 \tag{17}$$

i.e. a diffusion equation also for c_i with the same effective diffusion coefficient D_i^{eff}. Thus, the position 16 makes consistent the first and third Equation (14). Comparing with these equations, one infers that C_i and c_i must differ by a constant or coincide; the latter chance has particular interest as it agrees with the solenoidal character of the vector $c_iD_i\mathbf{v}_i$ previously remarked about Equation (10), which effectively justifies $C_i\equiv c_i$. Hence, it is possible to write

$$\frac{m_i}{kT}\frac{\partial\mathbf{v}_i}{\partial t}=-\frac{D_i^{\S}}{D_i}\frac{\nabla c_i}{c_i}+\frac{\mathbf{B}_i}{c_iD_i},$$
$$\nabla D_i^{\mathrm{eff}}\cdot\nabla c_i=\frac{\partial c_i}{\partial t}-D_i^{\mathrm{eff}}\nabla^2c_i \tag{18}$$

The first equation shows that the acceleration of the ith ion is controlled by the ratio $D_i^{\S}/D_i$ times the concentration gradient; the second equation defines D_i^{eff} as a function of the concentrations c_i. Thus the following equations hold

$$\nabla\cdot(c_iD_i\mathbf{v}_i)=0,\quad \mathbf{v}_i=\frac{kT}{m_i}\frac{D_i^{\S}}{\partial(c_iD_i)/\partial t}\nabla c_i \tag{19}$$

Note that Equations (18) and (19) are mutually self-consistent. Deriving with respect to time the divergence equation it must be true that $\nabla\cdot[\mathbf{v}_i\partial(c_iD_i)\partial t+c_iD_i\partial\mathbf{v}_i/\partial t]=0$, which is indeed verified. Deriving now $\mathbf{v}_i$ of Equation (19) with respect to time and comparing with $\dot{\mathbf{v}}_i$ of Equation (18), one finds

$$\frac{m_i\dot{\mathbf{v}}_i}{kT}=\frac{\partial}{\partial t}\left(\frac{\nabla c_i}{c_i}\frac{D_i^{\S}}{D_i}\frac{1}{\partial\log(c_iD_i)/\partial t}\right)=-\frac{\nabla c_i}{c_i}\frac{D_i^{\S}}{D_i}+\frac{\mathbf{B}_i}{c_iD_i}$$

The differential equation can be integrated in closed form to find the explicit expression of $D_i^{\S}/D_i$. It is easy to verify that the solution has the form

$$\frac{D_i^{\S}}{D_i}\frac{\nabla c_i}{c_i}=\left(\mathbf{A}_i+\int\mathbf{B}_i\,\mathrm{d}t\right)\frac{\partial(c_iD_i)}{\partial t}(c_iD_i)^{-2},$$
$$\mathbf{A}_i=\mathbf{A}_i(x,y,z) \tag{20}$$

The vector $\mathbf{A}_i$ is the time-integration constant having physical dimensions of mol $\times$ length^{-2}. Hence,

$$\mathbf{v}_i=\frac{kT}{m_i}\frac{\mathbf{A}_i+\int\mathbf{B}_i\,\mathrm{d}t}{c_iD_i},$$
$$\dot{\mathbf{v}}_i=\frac{kT}{m_i}\left(\left(\mathbf{A}_i+\int\mathbf{B}_i\,\mathrm{d}t\right)\frac{\partial(c_iD_i)^{-1}}{\partial t}+\frac{\mathbf{B}_i}{c_iD_i}\right),\quad(21)$$
$$\nabla\cdot\left(\mathbf{A}_i+\int\mathbf{B}_i\,\mathrm{d}t\right)=0$$

Equation (17) compels $\nabla\cdot\mathbf{A}_i=0$. Moreover, noting that $\dot{\mathbf{v}}_i=-\mathbf{v}_i\partial\log(c_iD_i)/\partial t+kT(m_ic_iD_i)^{-1}\mathbf{B}_i$ the first equation is directly verified. Both Equation (21) describe the dynamics of the ith ion in the solid oxide and show that $\mathbf{v}_i$ has the same direction as ∇c_i; as the gradient identifies the direction of greatest change of scalar field, it follows that the ion moves towards the maximum concentration difference. The acceleration has instead a different direction unless putting in particular $\mathbf{B}_i=0$, in which case the driving force on the left-hand side of Equation (16) would have a mere diffusive character. Note that the second Equation (18) defines the angle between the vectors $\nabla D_i^{\mathrm{eff}}$ and ∇c_i, which shows that even the maximum change of D_i^{eff} does not match the velocity vector. Hence, it is reasonable to conclude that the ion acceleration is affected by the gradients of both D_i^{eff} and c_i. In general, the acceleration and velocity with different orientations indicate that the ions do not move along a straight line. Clearly the concepts of 'straight' and 'curved' paths have mere statistical meaning, without any concern ofto the actual motion at the microscopic level. Yet it is reasonable to guess that in the case of an edge dislocation the ion motion lies on a plane parallel to the extra plane, because climbing along the Burgers vector would require more energy. The ion motion is expected to be more complex instead in the case of a screw dislocation because of its spiral shape. These remarks show that the vector $\mathbf{B}_i$ is directly related to the microstructure of the solid oxide. The vector $\mathbf{A}_i$ is now determined in order to fulfil a boundary condition of the problem. With regard to this point, note first that Equation (20) determines the ratio $D_i^{\S}/D_i$, which enables D_i^{eff}/D_i to be calculated by summing up with D_i^{*}/D_i of Equation (14). The key idea for this purpose still rests on the Nernst–Einstein equation, expressed however as a function of this D_i^{eff}. Since $\sigma_i^{\mathrm{eff}}=(kT)^{-1}(z_ie)^2c_iD_i^{\mathrm{eff}}$, it follows

$$\sigma_i^{\mathrm{eff}}=\frac{D_i^{\mathrm{eff}}}{D_i}\sigma_i,\quad \sigma_i=\frac{(z_ie)^2c_iD_i}{kT} \tag{22}$$

The ratio D_i^{eff}/D_i is therefore a multiplicative factor of the basic conductivity σ_i corresponding to the plain diffusion coefficient D_i without applied electric potential in a dislocation-free solid oxide. The second Equations (14) and (20) yield

$$\frac{\sigma_i^{\mathrm{eff}}}{\sigma_i}=\frac{z_ie\phi_{oi}}{kT}\alpha_i+\frac{|\mathbf{A}_i+\int\mathbf{B}_i\,\mathrm{d}t|}{(c_iD_i)^2}\frac{\partial(c_iD_i)}{\partial t}\frac{c_i}{|\nabla c_i|},$$
$$\sigma_{\mathrm{tot}}^{\mathrm{eff}}=\sum_j\sigma_j^{\mathrm{eff}} \tag{23}$$

Let the electric potential ϕ be switched on at $t=0$, so that $|\mathbf{A}_i+\int\mathbf{B}_i\,\mathrm{d}t|$ is determined in order to fulfil the boundary condition $\sigma_i^{\mathrm{eff}}\to\sigma_i^0=(z_ie)^2c_i^0D_i^0/kT$ at $t=0$; since the integral is defined as $\int_{t=0}^{t}\mathbf{B}_i(\tau)\,\mathrm{d}\tau$, then

with obvious meaning of symbols

$$A_i = \left(1 - \frac{z_i e \phi_{oi}^0 \alpha_i}{kT}\right)(c_i^0 D_i^0)^2 \frac{|\nabla c_i|_{t=0}}{c_i^0} \left(\frac{\partial (c_i D_i)}{\partial t}\bigg|_{t=0}\right)^{-1},$$

$$A_i = |\mathbf{A}_i|, \quad t = 0 \tag{24}$$

It will be shown below, see Equation (29), that $\phi_{oi} = \phi_{oi}(c_i)$ with $\phi_{oi}^0 = \phi_{oi}(c_i^0) = 0$; hence, D_i^0 being the diffusion coefficient in the solid oxide lattice in the absence of electric potential, as sketched in Section 2, Equation (24) suggests that $A_i = A_i(x, y, z)$ is related to the ion velocity at $t = 0$, i.e. according to Equation (21) $|\mathbf{v}_i^0| = kT(m_i c_i^0 D_i^0)^{-1} A_i$. Note at this point that all the formulae so far introduced are in some way expressed as a function of D_i, c_i, c_i^0 and ∇c_i. This is not surprising, rather this conclusion is a mere consequence of the number of equations and unknowns hitherto introduced. Once assuming known D_i and having defined α_i in the range $0.5 \leqslant \alpha_i \leqslant 1$, consider Equation (13) inferred from Equation (11) and including through the position 12 both the electric potential gradient and the stress field of the dislocation with which the ion carriers interact. In Equation (13) appear four unknown functions: the electric potential ϕ and $\mathbf{\Gamma}_i$ related to the functions ϕ_{oi}, the concentrations c_i, the drift velocities $\mathbf{v}_i$ of each ion; considering also the unknown functions $D_i^{\S}$ are in total 5. The equations available are 4: the Poisson Equation (2), the couple of Equation (19) and the diffusion Equation (18) that defines D_i^{eff}. The mathematical problem has therefore one redundant unknown function with respect to the number of equations, which introduces a freedom degree in determining one function of the problem; this redundancy allows to express the unknowns just mentioned as a function of c_i. The following considerations concern the way to find the concentrations c_i. As in general $c_i^{-1}\nabla c_i = \nabla \log(c_i/\gamma_i)$, with γ_i appropriate constants, Equation (12) gives

$$-\frac{\mathbf{\Gamma}_i}{c_i} + \frac{z_i e}{kT}\alpha_i \nabla\left(\phi + \frac{\mu_i}{z_i e}\right) = \frac{z_i e \phi_{oi}}{kT}\alpha_i \nabla \log\left(\frac{c_i}{\gamma_i}\right) \tag{25}$$

Define $\mathbf{\Gamma}_i$, not yet explicitly specified in Equation (12) as follows:

$$\frac{\mathbf{\Gamma}_i}{c_i} = \frac{z_i e}{kT}\alpha_i \log\left(\frac{c_i}{\gamma_i}\right)\nabla\phi_{oi} \tag{26}$$

This is the equation enabling c_i to be defined. Equation (25), combined with Equation (12), reads

$$\nabla\left(\phi + \frac{\mu_i}{z_i e}\right) = \nabla\left(\phi_{oi} \log\frac{c_i}{\gamma_i}\right) \tag{27}$$

The right-hand side of Equation (27) could be identically rewritten $\nabla[\phi_{oi}\log(c_i/\gamma_i) + \text{const}]$; thus, ϕ is defined as an arbitrary constant apart, as it must be, here put by definition equal to zero as emphasized in Section 2. With the given definition of $\mathbf{\Gamma}_i$, Equation (27) enables the electric potential ϕ to be calculated as a function of ϕ_{oi}

$$\phi = \phi_{oi}\log\left(\frac{c_i}{\gamma_i}\right) - \frac{kT}{z_i e}\log\left(\frac{c_i}{c_i^0}\right) \tag{28}$$

By definition ϕ is therefore the local potential due to the amount of charges flowing in a given point of the electrolyte at a given time. Let us now determine the functions ϕ_{oi} in order to fulfil the second and third Equation (2). Since $\nabla^2\phi$ involves a sum of concentrations, a reasonable form of ϕ_{oi} should be

$$\phi_{oi} = \left[\log\left(\frac{c_i}{\gamma_i}\right)\right]^{-1} \times \left\{\frac{kT}{z_i e}\log\left(\frac{c_i}{c_i^0}\right) + \sum_j \Phi_{0j}\log\left(\frac{c_j - c_j^0}{\gamma_j'}\right)\right\},$$

$$\gamma_j' = \gamma_j'(t) \tag{29}$$

where Φ_{0j} are constants having physical dimensions of electric potential. As the second Equation (2) gives

$$\phi = \sum_j \Phi_{0j}\log\left(\frac{c_j - c_j^0}{\gamma_j'}\right),$$

$$\nabla^2\phi = \sum_j \Phi_{0j}\nabla^2\log\left(\frac{c_j - c_j^0}{\gamma_j'}\right) = \sum_j q_j(c_j - c_j^0),$$

$$q_j = -\frac{z_j e}{\varepsilon_r \varepsilon_0} \tag{30}$$

the constants Φ_{0j} link the electric potential of the cell to the concentrations of charge carriers. The solution in closed form of Equation (30) for each ith ion is

$$c_i = c_i^0 + 2\Phi_{0i} q_i^{-1}\varphi^2[\tanh(\xi_i + \varphi_x x + \varphi_y y + \varphi_z z)^2 - 1],$$

$$\varphi^2 = \varphi_x^2 + \varphi_y^2 + \varphi_z^2 \tag{31}$$

where φ_x, φ_y, φ_z and ξ_i are x-, y-, z-integration constants. Regard, therefore, them as follows:

$$\varphi_x = \varphi_x(t), \quad \varphi_y = \varphi_y(t), \quad \varphi_z = \varphi_z(t), \quad \xi_i = \xi_i(t),$$

$$\varphi_x(t=0) = \varphi_y(t=0) = \varphi_z(t=0) = 0 \tag{32}$$

Equation (32) fulfils the boundary condition $c_i = c_i^0$ for any x, y, z at $t = 0$. Equations (31) and (32) are useful in particular to describe the charge flows in electrolytes interested by multi-ion conduction mechanism, where ions of opposite charges move towards opposite directions depending on the electrode where they are generated; for instance, H^+ moves from anode to cathode, whereas O^{-2} moves from cathode to anode. One expects therefore that the concentration profile along the z-axis of positive ions decreases from the anode where they are generated to the cathode, whereas the opposite holds for negative ions. This holds for any coordinates x and y, which suggests introducing one $x \div y$ plane for instance at $z = 0$ defined as electrolyte boundary; also, it seems reasonable to fix a further electrolyte boundary on a plane at $z = z_o$ parallel to the former. Clearly these planes identify the interfaces between the electrolyte of thickness z_o and the

electrodes. Equation (31) describes therefore the concentration profile of positive and negative ions flowing through the solid oxide if written more expressively as follows with obvious meaning of symbols

$$c_l^- = c_l^0 + 2\Phi_{0l} q_l^{-1} \varphi^2 [\tanh(\xi + \varphi_x x + \varphi_y y + \varphi_z z)^2 - 1], \quad 0 \leqslant z \leqslant z_o, \quad \xi \equiv \xi_i \tag{33a}$$

$$c_k^+ = c_k^0 + 2\Phi_{0k} q_k^{-1} \varphi^2 [\tanh(\xi + \varphi_x x + \varphi_y y - \varphi_z z')^2 - 1], \quad z' = z_o - z, \quad 0 \leqslant z' \leqslant z_o, \quad \xi = \xi_i - z_o \tag{33b}$$

The indexes l and k refer to any ions of the respective signs. Both Equation (33) are solutions of Equation (30); they simply rewrite Equation (31) in order to emphasize that z' changes from z_o to 0 when z changes from 0 to z_o. Clearly the thickness of electrolyte z_o is an input of the problem. It is now possible to calculate Equation (24); trivial calculations show that

$$\frac{|\nabla c_i|}{\partial c_i / \partial t} = \frac{\varphi^2 \tanh(\chi)}{\dot{\varphi} - \varphi \dot{\chi} \tanh(\chi)}, \quad \chi = \xi + \varphi_x x + \varphi_y y + \varphi_z z \tag{34}$$

In general, the ratio on the left-hand side is a function of x, y, z, t that defines a differential equation involving $\dot{\chi}$ and χ. Here we are interested in particular in the limit required by Equation (24). As $A_i \neq 0$, otherwise according to Equation (21) the ions would be at rest at $t = 0$, Equation (24) compels the existence of a finite value for $|\nabla c_i|_{t=0} (\partial c_i / \partial t)|_{t=0} = r(x, y, z) \neq 0$ that at this limit must agree with $\varphi \to 0$ too. This condition is fulfilled determining appropriately the time profiles of ξ and φ_x, φ_y, φ_z, not yet specified. Assume without loss of generality that in agreement with Equation (32) $\dot{\varphi}_x$, $\dot{\varphi}_y$, $\dot{\varphi}_z$ tend to zero, whereas $\dot{\xi}$ does not; then $\dot{\chi}$ tends to $\dot{\xi}$ for $t \to 0$, so that in this limit the right-hand side of Equation (34) reduces to a differential equation containing the time only. This differential equation integrated in closed form yields

$$\varphi = \frac{r(x, y, z) \cosh(\xi)}{\int_0^t \sinh(\xi)\, \mathrm{d}\tau}, \quad t \to 0$$

One verifies that if $\xi(t)$ tends to infinity for t tending to zero, for instance like $1/t$, then φ tends to zero, as required by Equation (32); this does not cause any divergence problem in Equation (31) because $\tanh(\infty)=1$ for $t \to 0$, whereas the time profile of ξ confirms that effectively χ reduces to ξ in this limit. In conclusion, noting that ϕ_{oi} of Equation (29) tends to zero, Equation (24) yields

$$r(x, y, z) = \frac{|\nabla c_i|_{t=0}}{\partial c_i / \partial t|_{t=0}}, \quad A_i = c_i^0 D_i^0 r(x, y, z) \tag{35}$$

Hence $r(x, y, z)$ is nothing else but the function related to the modulus of the vector $\mathbf{A}_i$ introduced above; if for instance the components of $\mathbf{A}_i$ have the form $A_{xi} = A_{xi}(y, z)$, and analogously for the other components, then $r(x, y, z)$ can be regarded as the modulus of the vector $\mathbf{r}(x, y, z)$ having components $r_x = r_x(y, z)$ and so on. The function $\mathbf{B}_i$ is determined thanks to the continuity condition, which is therefore fulfilled even though the ion motion does not have a mere diffusive character. With the mass flow $c_i \mathbf{v}_i$ calculated by means of Equation (21), Equation (2) yields

$$\frac{kT}{m_i} \frac{\left(\mathbf{A}_i + \int \mathbf{B}_i\, \mathrm{d}t\right) \cdot \nabla c_i}{D_i^2} = \frac{\partial c_i}{\partial t}$$

In principle $\mathbf{B}_i$ defined by this equation can be calculated by means of standard computational techniques once knowing $\mathbf{A}_i$. Let us justify now why γ_i' have been introduced in Equation (29) as time functions rather than as mere constants. Consider that $c_i \to c_i^0$ for $t \to 0$; hence, divergent terms would appear in the potential expression of Equation (30). Yet, if in this limit $\gamma_i' \to 0$ as well, the log term remains finite even at $t = 0$. It is easy to verify that this happens if γ_i' tends to zero like $\gamma_i' = \eta_i \varphi^2 (\tanh(\xi)^2 - 1)$ with η_i arbitrary coefficients. If so, the limit of ϕ for $t = 0$ is given by $\sum_j \Phi_{0j} \log(2\Phi_{0j} q_j^{-1} \eta_j^{-1})$. A proper choice of the coefficients Φ_{0i} such that $2\Phi_{0j} = \eta_j q_j$ fulfils thus $\phi(t = 0) = 0$, as required. Moreover the fact that $\phi > 0$ is related to values $c_i > c_i^0$ allows a correct choice of γ_i according to Equation (29): terms like $\log((c_j - c_j^0)/\gamma_j')$ $\log(c_i/\gamma_i)$ never diverge if $\gamma_i < c_i^0$, while it also follows that ϕ_{oi} tend to zero at $t = 0$. Note now that the time does not enter explicitly in Equation (31), but through the functions φ_x, φ_y, φ_z and ξ only; then nothing hinders to define these functions in order that they vanish also at an arbitrary time t_{end}, for which hold all the considerations carried out for $t = 0$. In particular it is true that $c_i(t_{\mathrm{end}}) = c_i^0$, so that $\phi(t_{\mathrm{end}}) = 0$ as well, while holding again the consequences of Equation (34), i.e. Equation (35) and $\phi_{oi} = 0$ at $t = t_{\mathrm{end}}$ as well; thus one must have to this purpose $\xi(t) \propto t^{-1}(t_{\mathrm{end}} - t)^{-1}$. With this boundary condition the various c_i describe an ideal thermodynamic cycle of a perfectly reversible electrochemical cell that starts working at $t = 0$ and is switched off at $t = t_{\mathrm{end}}$, while the concentrations of charge carriers having initial values c_i^0 increase to c_i when the electrochemical reaction generates energy and then returns back exactly to their initial values c_i^0 when the cell stops working. In agreement with the boundary conditions at the times corresponding to ramp up and ramp down of the cell power, ξ was defined in order to tend to infinity; yet at intermediate times ξ can be determined in order to give a prefixed time profile of both concentrations and potential. Clearly the time profile of the function ξ is an input of the simulation problem. Moreover, the functions φ_x, φ_y, φ_z control how the ion concentrations occur in various points of the electrode/electrolyte interface; for instance $\varphi_x = \varphi_y$ entails $c_i(x, y, z, t) = c_i(y, x, z, t)$ i.e. x,y symmetry at any z,t; instead $\varphi_x = \varphi_y = 0$ and thus $\varphi^2 = \varphi_z^2$ describe a one dimensional flow of charges and so on. Clearly φ_x, φ_y, φ_z are also input functions, i.e. freedom degrees of the model that allow a wide variety of operating conditions of the cell to be simulated. The positions above, in particular Equation

(28), help to calculate the effective diffusion coefficient that determines each ion drift velocity and thus, via Einstein's equation, the characteristic conductivity as well. According to Equation (14) and (28)

$$\frac{D_i^*}{D_i}=\alpha_i\left[\log\left(\frac{c_i}{\gamma_i}\right)\right]^{-1}\times\left\{\log\left(\frac{c_i}{c_i^0}\right)+\sum_j\frac{\Phi_{0j}z_je}{kT}\log\left(\frac{c_j-c_j^0}{\eta_j\varphi^2\left(\tanh(\xi)^2-1\right)}\right)\right\} \tag{36}$$

So, thanks to Equations (20), (21) and (23), the effective conductivity due to the ith ion reads

$$\frac{\sigma_i^{\text{eff}}}{\sigma_i}=\alpha_i\left[\log\left(\frac{c_i}{\gamma_i}\right)\right]^{-1}\times\left\{\log\left(\frac{c_i}{c_i^0}\right)+\sum_j\frac{\Phi_{0j}z_je}{kT}\log\left(\frac{c_j-c_j^0}{\eta_j\varphi^2\left(\tanh(\xi)^2-1\right)}\right)\right\}+\frac{m_i|\mathbf{v}_i|}{D_ikT}\frac{\partial(c_iD_i)/\partial t}{|\boldsymbol{\nabla}c_i|} \tag{37}$$

This expression is easily calculated as a function of c_i with the help of Equation (34) and (35). Note that $\sigma_i^{\text{eff}}/\sigma_i$ consists of three addends: the first two are monotonic increasing functions of c_i, the third one is proportional to the ion velocity and additive to the former two; as it must be true that σ_i^{eff} increases with the velocity of the ion, the positive sign of the time derivative is required for increasing values of c_i. In effect this conclusion, self-evident if D_i is approximately constant, is in general fulfilled determining appropriately the constants Φ_{oi} of Equation (33) and the functions φ_x, φ_y, φ_z and ξ to establish the correct sign of $\dot{\varphi}-\varphi\dot{\chi}\tanh(\chi)$ in Equation (34). According to Equation (23), therefore, enhanced conductivity during service life of the cell with respect to the characteristic initial value of the solid oxide is to be expected as a function of the local values of c_i and c_i^0 because $D_i^{\S}+D_i^*>D_i$ for $c_i>c_i^0$. To calculate the power supplied by the cell note that $\phi^2\sigma$ has physical dimensions of power per unit length; so, if S is the surface of plane electrodes z_o apart, one finds

$$W=S^{-1}\int\int_S \mathrm{d}x\,\mathrm{d}y\int_0^{z_o}\phi^2\sigma_{\text{tot}}^{\text{eff}}\,\mathrm{d}z,\qquad \phi=\sum_j\Phi_{0j}\log\left(\frac{c_j-c_j^0}{\eta_j\varphi^2\left(\tanh(\xi)^2-1\right)}\right) \tag{38}$$

The integral on z takes into account the concentration profile of the various ions that reach the electrode after having travelled through the electrolyte, which gives the power corresponding to one of these paths in a given point of the electrode boundary; the surface integral averages this power over the paths of ions generated everywhere in the respective electrodes. Thus the formula yields the average power due to all ions that flow in the cell under electric potential profile controlled by the input time function ξ and by the coefficients η_i. These Appears in this result the link between physico-chemical properties and performances of the electrolyte; in summary, the correlation stems from the concentrations c_i^0 and c_i controlling: (i) the electrolyte conductivity σ_i^{eff} through D_i^{eff}, (ii) the electric potential ϕ and (iii) the total power W consistent with the amount of charge carriers flowing in the electrolyte. Also, Equation (28) highlights the correlation between c_i and the electrochemical potential $\phi_{ec}=\phi+\mu_i/z_ie$ of each charge carrier, with μ_i introduced in Equation (8); this means that the ion concentration profiles within the electrolyte are controlled by ϕ_{ec} and by consequence W depends on how the ions spread crossing the electrolyte through the integrand factor $c_i-c_i^0$. The present model was focused mostly on the charge transport in the electrolyte; yet the performances of the whole cell clearly depend also upon the environment experienced by the ions crossing the cathodic and anodic materials and upon the properties of the respective electrode/electrolyte interfaces.

4. DISCUSSION

A full model of ionic conductivity should start from the physico-chemical properties of the solid oxide electrolyte (dopant composition, crystal symmetry, grain size, nature of the grain boundaries and so on) to calculate the performances of a fuel cell under well-defined working conditions, e.g. at a given temperature. This ultimate task implicitly assumes known the physical link between microstructural properties of the solid oxide and mobility and concentration profiles of the charge carriers. Actually this correlation has been sketched in principle only; the Darken equation was introduced in section 2 just to highlight shortly how the microstructure of the solid oxide enters into the problem through D_i, yet without detailed considerations at the microscopic level about the sought link for each ion. The same holds for the velocity and acceleration of the ions defined in Equation (21) as a function of c_i. It has been emphasized that the local value of D_i depends on c_i because the presence of an increased concentration of ions crossing the lattice affects the global amount of crystal defects, which explains why in principle $D_i^0\neq D_i$ and justifies the concept of effective diffusion coefficient D_i^{eff} in the presence of dislocations and electric potential too. In practice, however, Equation (37) can be calculated putting as a first approximation $D_i\sim D_i^0$, which is justifiable if c_i do not deviate too much from c_i^0. Moreover, A_i defining the ion velocity in Equation (24) have been calculated as a consequence of the position of Equation 16, thus concluding that the edge or screw character of the dislocation affects the conductivity through D_i^{eff}. Hence, the model makes

explicit reference to the microstructural aspects of the problem, in particular about the correlation between D_i^0 experimentally measurable and D_i function of c_i. Clearly investigating this topic would require a separate micro/nano-scale theoretical model propaedeutic or complementary to the calculation scheme so far described and utilizing an approach conceptually different; otherwise stated, including the micro-scale aspects of the global problem in the present context would compel merging together two models intrinsically dissimilar. So the mathematical scheme outlined in Section 3 merely aims to show the correlation between the main parameters characterizing the ion conduction in a solid oxide electrolyte, whose microstructure remains however hidden in the macroscopic parameter D_i assumed known '*a priori*' and thus necessarily regarded as input information. Nevertheless, the model accounts for how ion velocity and concentration affect the conductivity, see Equations (22) and (37). It is worth noticing in this respect that usually the Fick equation is solved for the concentrations to calculate the amount of charge flowing through the electrolyte. Here this standard approach is in fact reversed. Rather than speculating on how to formulate $D_i^{\text{eff}} = D_i^{\text{eff}}(c_i, \phi, \mathbf{F})$ and solve by consequence the Fick equation, the model introduces first the perturbation induced by the lattice defects on the ions moving under a given electric potential; the diffusion-like behaviour of the ion is then required by necessity because of the concentration gradients expected for ions travelling through the electrolyte from one electrode to the other. Equation 33 calculated at $t>0$ as a function of z or z' depending on the charge of the ion at any x, y show decreasing z-profiles between the boundaries of the electrolyte, the highest concentration being of course at the interface with the electrode where the ion is generated. The effective diffusion coefficient is therefore identified by definition as the function of c_i and ϕ that makes the force field of Equation (9) consistent with the known form of the Fick equation. In effect, the positions of Equations (9) and (26) replace the microscopic stress field of dislocation shortly sketched in Section 2, whereas the electro-chemical potential, on the left-hand side of Equation (27), is a by consequence of the expected driving energy of the cell. The main peculiarity of any macroscopic approach is that average statistical quantities, e.g. temperature or diffusion coefficient, replace microscopic details difficult to be modelled without valid hypotheses and drastic simplifying assumptions; so the present approach introduces in a natural way the crucial concept of temperature dependence of ion conductivity simply thanks to the Nernst-Einstein equation that contains the factor kT. The information provided by this equation includes at least three points: (i) the conductivity is not the same everywhere in the solid oxide, as it depends on the local value of ion concentration c_i; (ii) it is immediate to describe as a function of the temperature the most significant working parameters of a fuel cell, i.e. ion conductivity and total power of the cell; (iii) drift speed, acceleration and concentration of the ions appear mutually correlated according to Equation (21). In the characteristic way of any thermodynamic model, the available information concerns essentially the energy balance of the whole process, regardless of the microscopic details: the Fick and Nernst-Einstein equations and the continuity condition are proven enough to bypass the detailed knowledge of the local microstructure. Thanks to these equations elementary considerations avoid preliminary hypotheses about how electric potential and lattice defects determine the effective diffusion coefficient; even without carrying out explicit numerical calculations D_i^{eff} is found to depend on the local mobility and concentration of the ions, thus confirming that effectively the lattice defects actually related to the presence of these ions control the performances of the cell. Neglecting the lattice strain field around one vacancy, the diffusion process is quite simply accounted for in both cases of ideal crystal and real crystal: either case being essentially controlled by jump frequency and activation energy, the problem regards the diffusion coefficient only. In the presence of dislocations the problem is more complex, because the stress field affects the neighbouring lattice for the reasons sketched in section 2; in particular, the long range action changes the chance of accommodating ions in zones squeezed by the extra plane. Ions climbing an edge dislocation and ions travelling alongside its extra plane cannot be described simply changing their jump frequency and activation energy, as the vector character of the stress introduces preferential directions of motion in the lattice intuitively related to the Burgers vector. It is not surprising therefore that the considerations about Equation (16) compel remarking the edge or screw character of the dislocations, as either of them entails a different kind of long range action and thus a different expression of ion velocity inside the electrolyte. Hence, the lack of microstructural information is a feature of the model rather than a conceptual incompleteness; it simply suggests the usefulness of formulating a micro-scale model, at the moment in progress, to valuably implement the physical information hitherto outlined. The strategy of focusing on the correlation between ion mobility and concentration while skipping the microstructure of the solid oxide, on the one side greatly simplifies the formulation of the mathematical model; on the other side it also suggests how to extend the model, initially conceived under the simplifying assumptions of infinite and isotropic single crystal of solid oxide, to the case of a real polycrystalline material with grain boundaries too. It is known that the physico-chemical properties of these latter differ from that of the grain bulk by chemical composition (e.g. because of grain boundary segregation), amount

Int. J. Energy Res. 2011; **35**:1056–1074 © 2011 John Wiley & Sons, Ltd.
DOI: 10.1002/er

of stresses (e.g. because of the mismatch between grains with different orientations), amount of defects (e.g. vacancies and voids because of the altered local stoichiometry and fast grain growth in non-equilibrium conditions) and so on; if all these properties affect the ion diffusion, as it is reasonable to expect, the microstructural properties of grain boundaries or nano-phased materials can be taken into account by simply changing appropriately the values of D_i^0 and c_i^0 in selected zones of a single crystal that correspond to the presence of grain boundaries with the desired physico-chemical properties. The model has initially assumed that the values of D_i^0 and c_i^0 are constant everywhere in the crystal, which appears therefore as an infinite body of homogeneous matter. Yet, exploiting the fact that $D_i = D_i(c_i)$ and $D_i^{\text{eff}} = D_i^{\text{eff}}(c_i)$, it is possible to delineate grain boundaries in a single crystal introducing local values of D_i^0 and c_i^0 purposely altered in order to simulate their distinctive space charges and defects; Figure 1 sketches schematically an ideal cross section of the solid oxide emphasizing the presence of grain boundaries that in turn outline various crystal grains. In a macroscopic model this means regarding the grain boundaries simply as peculiar zones of solid oxide characterized by their own initial composition and microstructure. Recall in this respect the possibility of regarding $\mathbf{A}_i$, by definition a basic property of the solid oxide in the absence of electric potential, as a constant vector or as a vector uniquely defined as a function of the coordinates. In the former case $\mathbf{A}_i$ are mere simulation parameters that enter into the problem of an infinite single crystal, in the latter they are functions of space coordinates able to describe grains of desired size and grain boundaries of desired width; the coordinate dependence of $\mathbf{A}_i(x, y, z)$ corresponds in this way to the zones of solid oxide where it is defined the anomalous values of D_i^0 and c_i^0. While in principle the mathematical model remains basically the same, the main task is how to define appropriately the new local values in order that they represent correctly the chemistry of the grain boundaries. In this respect it appears especially useful the aforesaid micro/nano-structural model, whose formulation is clearly motivated and outlined by the present results. Once having emphasized the role of point and line lattice defects on the ionic conductivity, the model stimulates further considerations based on elementary concepts of electrochemistry and solid-state physics. It is known that sliding and pile-up of tangled dislocations at the grain boundaries typically occur under mechanical and thermal stresses of sintering and that the dislocation flow occurs preferentially along definite crystal planes; TEM observations have confirmed the occurrence of this flow, see for instance [18] for Al_2O_3 whose slip system is $[0001]\langle 11\bar{2}0\rangle$[19]. In ceramics, dislocation pinning is also allowed to occur by solute atoms and at the grain boundaries that act as a barrier to gliding [20]; tangled dislocations form by consequence. Moreover, the interaction of ions with the grain boundary defects appears also significant; for instance it has been experimentally found that hydrogen is trapped by tangled dislocations in Fe [21], which prospects the reasonable possibility that other ions also could exhibit an analogous behaviour even in ceramics. These considerations have general character; whatever the specific kind of solid oxide and its initial microstructure might be, they allow to guess the environments experienced by an ion moving from the grain bulk towards a neighbor grain. Excluding for simplicity possible micro-voids or micro-cracks one expects: first a pile-up layer of tangled dislocations facing the grain boundary, then the different elemental and defect concentration typical of the grain boundary itself and subsequently an analogous situation reversed in the next grain. However well-known materials processing techniques suggest a possible chance to enhance the transport properties through the boundary layers, e.g. rearranging the tangled dislocations through appropriate annealing heat treatments leading to ordered arrays of dislocations via polygonization mechanism; such a process, well known in physical metallurgy, is described in [22] for Al_2O_3, whereas stacking fault annihilation and grain growth in ß-SiC is reported in [23]. Despite this, the actual grain boundary physics appears far more complicated than that of defect-free ideal grains, and so the ion transport mechanisms through these boundary layers as well, the calculation plan previously outlined can be similarly replicated if it is known or at least somehow hypothesized the local input values of $c_{i,gb}^0$ and $D_{i,gb}^0$

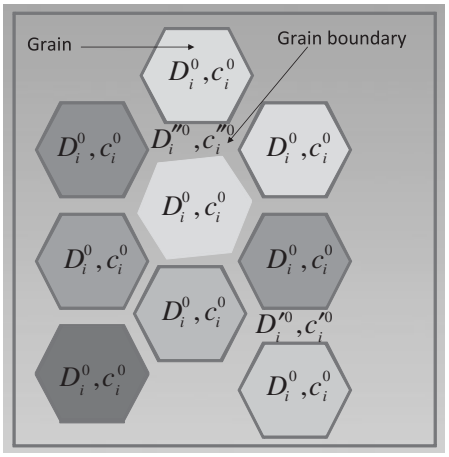

Figure 1. Schematic view of grains and grain boundaries on an ideal cross section of a polycrystalline solid oxide. The input data of the model, D_i^0 and c_i^0, are shown in various zones of the figure with notations emphasizing possible inhomogeneities of the solid oxide that segregate at the grain boundaries. The input values in general differ from point to point of these latter because of the diffusion coefficient-driven segregation, in turn dependent on the orientation of the crystal planes with respect to the cross section.

replacing $c^0_{i,\mathrm{core}}$ and $D^0_{i,\mathrm{core}}$; these latter are nothing else but c^0_i and D^0_i of section 3 rewritten with notation that emphasizes their meaning of grain core property. For instance one could guess $c^0_{i,gb} > c^0_{i,\mathrm{core}}$ if the aforesaid 'trapping effect' of tangled dislocations is really operating, in which case the reduced mobility of the ith carrier in the local stress field of dislocation network would require $D^0_{i,gb} < D^0_{i,\mathrm{core}}$. A practical difficulty to quantify these ideas arises from the lack of selective experimental data that define the former couple of grain boundary input values from which $c_{i,gb}$ and $D^{\mathrm{eff}}_{i,gb}$ could be in principle calculated. The importance of micro-scale models able to calculate '*ab initio*' the missing input data for any solid oxide/dopant system is thus highlighted by the ability of the present model to motivate and indicate specifically the kind of information necessary to proceed further with macro-scale calculations; quantifying the possible reasons that entail $D^{\mathrm{eff}}_{i,gb} < D^{\mathrm{eff}}_{i,\mathrm{core}}$ means indeed understanding the mechanisms that unfortunately compel $\sigma^{\mathrm{eff}}_{i,gb} < \sigma^{\mathrm{eff}}_{i,\mathrm{core}}$. Note eventually that in any case the model can also be exploited in a self-consistent way, e.g. fixing a series of arbitrary initial values of $c^0_{i,gb}$ and $D^0_{i,gb}$ in agreement with the inequalities above to simulate how much various levels of grain boundary segregation affect the grain boundary conductivity; in this way, comparing the calculated power with the experimental values provides indirect information about the grain boundary defect system. Of course these results can be repeatedly obtained at various temperatures by simply setting pertinent values of the factor kT that appears in the formulae above. In conclusion, the solution of the system of Equation (2) provides one with a road map to predict the ion transport in the solid oxide before and after appropriate heat treatments enabling point and line lattice defects designed in order to optimize the performances of ITSOFCs. A systematic computer simulation of the results so far obtained is at present in advanced progress in parallel with the development of a further micro/nano-scale model.

5. PRELIMINARY SIMULATION TESTS

Let i regard for simplicity of two ions of opposite sign only. The preliminary simulation tests concern the concentration profiles c_i/c^0_i of these ions at $x = 0, y = 0$ as a function of the ratio $0 \leqslant z/z_o \leqslant 1$ and at $y = 0$ as a function of x/x_o for selected values of z/z_o; the arbitrary length x_o expressing the x-coordinate in a dimensionless way is introduced simply defining $\varphi_x = \varphi'_x(t)/x_o$ in Equation (31). The following considerations on the concentration profiles are important because the concentrations are just the starting points to calculate the consequent values of D^{eff}_i and σ^{eff}_i by standard numerical procedures. Before showing that the results are useful here are some remarks to clarify what to expect from the simulation. The first remark is that Equation (33) have a maximum as a function of x at any z and y given by $x^{\max}_1 = -(\xi + y\varphi_y + z\varphi_z)/\varphi_x$ and $x^{\max}_2 = -(\xi + y\varphi_y + (z_o - z)\varphi_z)/\varphi_x$; hence, when calculating for instance the x-profile of the ion 1, one expects at any time a bell-shaped curve whose maximum shifts along the x axis as a function of z from $-(\xi + y\varphi_y)/\varphi_x$ to $-(\xi + y\varphi_y + \varphi_z)/\varphi_x$. If φ_z is positive, Equation (33) describe the peak positions of the ion displacing leftwards as long as it crosses through the electrolyte; if instead φ_z is negative, the concentration peaks shift rightwards. It is reasonable to regard the maximum concentration of the bell-shaped curve as the most probable position of the ion, i.e. its chance to pile up somewhere in the lattice. In both cases the concentration x-profiles indicate a confinement mechanism in the presence of dislocations: from a mathematical point of view, however, this really happens when the input function φ_x is chosen large enough to have $x\varphi_x \gg \xi$ at increasing values of x; if instead φ_x is so small to have $x\varphi_x \ll \xi$ for a large range of values of x then the x-profiles are flat, i.e. c_i depend so weakly upon x that the concentration peak in fact disappears. In the former case the confinement effect is operating, in the latter case it does not. The preliminary simulation tests reported below aim to explain the physical meaning of these features of c_i that, in agreement with the behaviour of the ion in the lattice, have a dynamical character because of the time dependence of the functions of Equation (31). Note in this respect that the solution of the second Equation (30) can also be expressed as follows

$$\begin{aligned} c_i &= c^{(1)}_i(\xi^{(1)}, \varphi^{(1)}, \varphi^{(1)}_x, \varphi^{(1)}_y, \varphi^{(1)}_z) + \alpha c^{(2)}_i \\ &\quad \times (\xi^{(2)}, \varphi^{(2)}, \varphi^{(2)}_x, \varphi^{(2)}_y, \varphi^{(2)}_z), \\ c^0_i &= c^{0(1)}_i + \alpha c^{0(2)}_i \end{aligned} \tag{39}$$

where α is a proper coefficient and each $c^{(j)}_i$ has the form of Equation (31); it holds of course the relationship $(\varphi^{(j)}_x)^2 + (\varphi^{(j)}_y)^2 + (\varphi^{(j)}_z)^2 = (\varphi^{(j)})^2$ for both terms. Let $\varphi^{(1)}_z$ be positive and $\varphi^{(2)}_z$ negative. The first term of the linear combination alone describes the ion displacing leftwards at increasing z, the second term alone the ion displacing rightwards; the linear combination of both terms suggests therefore the possibility of describing, with appropriate α, ions confined between two potential barriers in the lattice and thus moving statistically straightforward from one electrode to the other under electric potential gradient. These features of Equation (39) are not mathematical artefacts, they can be understood with reference to the explicative Figure 2 that highlights the chance of the ions to be piled up in the presence of dislocations. Consider first two edge dislocations only, imagined for simplicity crossing through the electrolyte, arbitrarily apart and

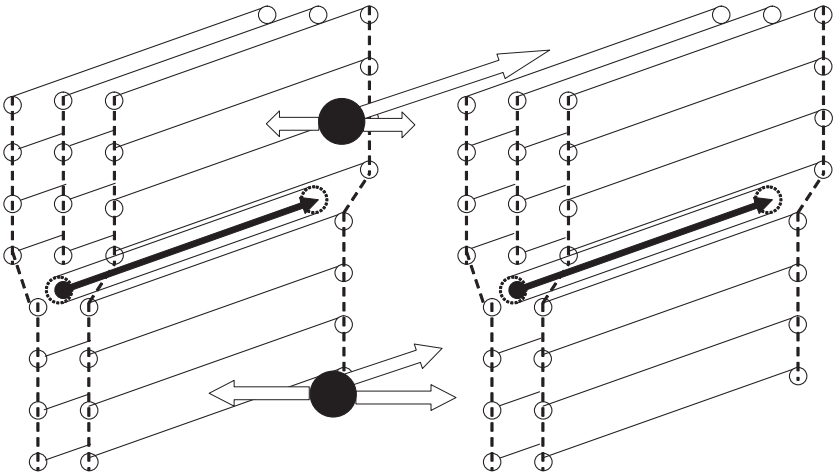

Figure 2. Schematic view of two edge dislocations oriented along a common direction. The figure shows how two ions moving normally to the Burgers vector can be channelled in the stretched zone and in the stress field of the extra-planes.

with extra-planes oriented perpendicularly to the anodic and cathodic interfaces. This figure suggests two possible ion confinement mechanisms: small ions, e.g. typically H^+ are likely to tunnel in the stretched zone towards the opposite electrode; moreover, the high energy necessary for heavier ions to climb above the dislocation extra-planes makes less probable their spreading through the most favourable crystal planes of the lattice. Both mechanisms of confinement appear advantageous for the overall efficiency of charge transport, because the channelling tends to reduce the ion scattering far from the most straightforward path between the electrodes. Hence, Figure 2 concerns a heavy ion bouncing rightwards and leftwards by effect of the boundary stress fields; it also shows an ion at the bottom that interacts weakly with the dislocation or, depending on its real position, does not interact at all. Clearly the ability of the linear combination of Equation (39) to balance and combine into a resulting concentration profile the ion propensity to both lateral displacements previously evidenced at different z, should also consequently ensure the average straightforward path between the electrodes. Moreover, the y dependence of c_i, for which hold of course the same considerations carried out for the x axis, accounts for similar effects along the third dimension as well; so the x-confinement suggested by Figure 2 can actually turn into an even more efficient x,y effect in the realistic case of a 3D array of several dislocations sketched schematically in Figure 3, well known and experimentally observed. As noted before, the values of φ_x and φ_y of Equation (31) enable to switch on or off the confinement effect just described: clearly flat x-profiles are consistent with extra planes of the dislocations of Figure 2 oriented normally to the electric potential driven ion flow, which prevents both confinement mechanisms. This also shows that the way to define the input time profiles of φ_x and φ_y with

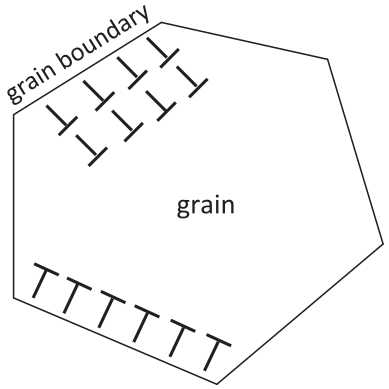

Figure 3. Schematic view of an array of grain boundary edge dislocations formed from tangled dislocations after polygonization heat treatments.

respect to ξ is actually representative of the average orientation of the Burgers vector with respect to the ion flow. Finally, Figure 2 suggests itself that the average information provided by the present model must statistically account not only for the chance of ion confinement but also for the chance that the confinement mechanism is not effective, even though in principle allowed, for ions travelling far from the dislocation stress field. Hence, together with the possible existence of bell-shaped profiles, one also expects $c_i > c_i^0$ everywhere in the electrolyte; indeed the concentration boost is anyway indicative of electric potential $\phi > 0$ and working condition of the cell even if some among the ions interact weakly or not at all with the dislocations. In fact, Figures 4–7 show the results of simulation carried out through Equation (39) that verify all of the features of c_i hitherto concerned. Figure 4 shows the concentration profiles c_i/c_i^0 at $x = 0, y = 0$ vs z/z_o; the profiles have been calculated

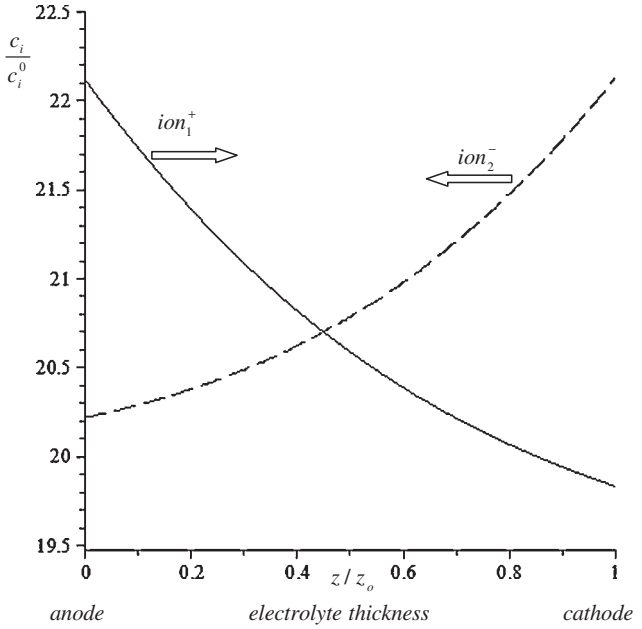

Figure 4. Concentration profiles of positive and negative ions at $x = 0, y = 0$ calculated through Equation (39) vs z/z_o. The z axis is normal to the interface planes between the electrodes. The trial values of the time functions, here introduced as fixed simulation parameters at one arbitrary time, are equal for both ions: $\xi^{(1)} = \xi^{(2)} = 1$, $\varphi_x^{(1)} = \varphi_x^{(2)} = 1$, $\varphi_y^{(1)} = \varphi_y^{(2)} = 2$, $\alpha = 6$; moreover, $\varphi_z^{(1)} = 1$, $\varphi_z^{(2)} = -0.01$. The parameter $a = \pm 1$ summarizes all constant factors appearing in Equation (31).

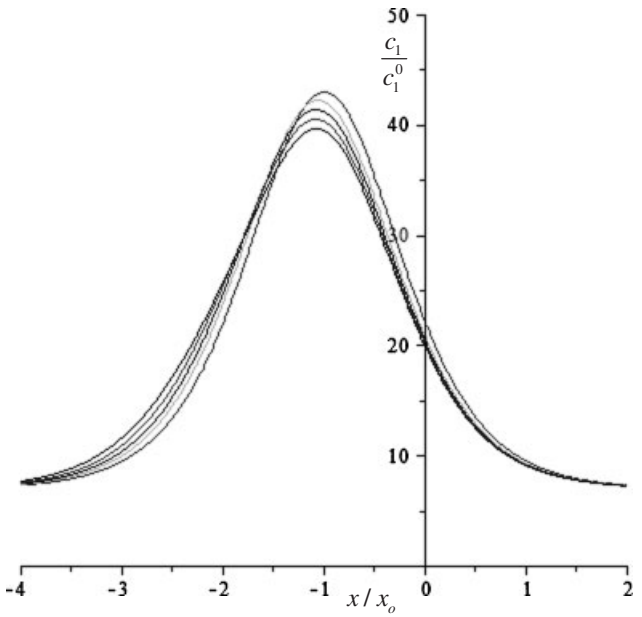

Figure 5. Concentration profiles of the ion 1 of Figure 4 as a function of x at $y = 0$ calculated with Equation (39). The x axis is defined on the interface plane between electrode and electrolyte perpendicularly to the z axis.

assigning arbitrarily trial values to the time functions ξ, φ_x, φ_y, φ_z to emphasize in the simplest way the kind of information provided by the model. The simulation parameters are quoted in figure. As expected, the anion generated at the anode has a decreasing profile while migrating towards the cathode; the same occurs for the cation travelling from the opposite electrode. More interesting are the x-profiles calculated at any y for various values of z/z_o. To simplify the graphic presentation of the results, we still assume $y = 0$ to visualize 5 profiles of c_i/c_i^0 vs x/x_o for as many selected values of z/z_o; an appropriate choice of x_o makes the

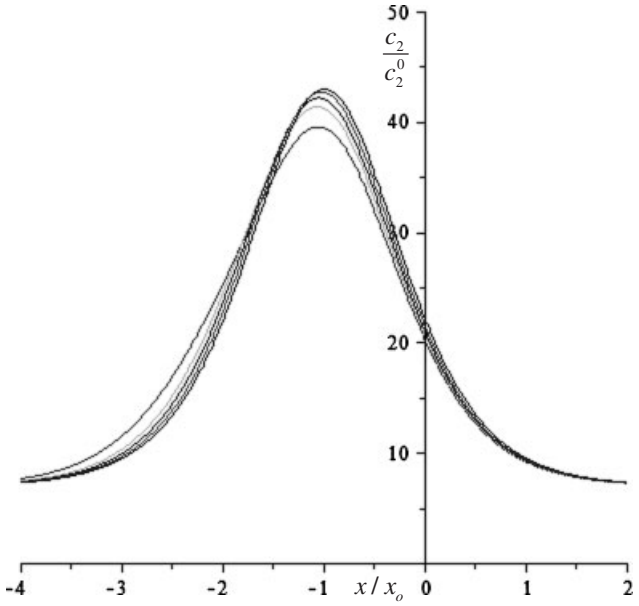

Figure 6. Same as Figure 5 for the ion 2 of Figure 4. Also in this figure the functions $\varphi_x^{(1)}$ and $\varphi_x^{(2)}$ of anion and cation are equal. Because of this simulation choice, the peak of the ion represented here coincides with that of Figure 5.

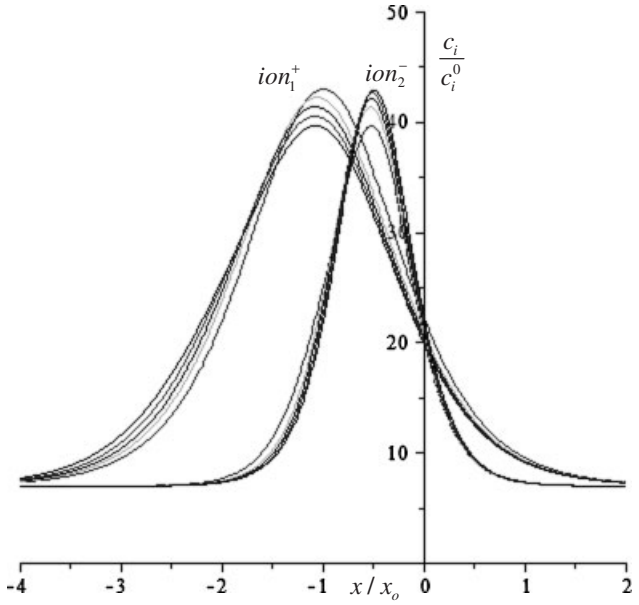

Figure 7. Concentration x-profiles of the ions of Figure 4 calculated with Equation (39). Here the functions $\varphi_x^{(1)}$ and $\varphi_x^{(2)}$ of anion and cation are different: for the cation $\varphi_x^{(1)} = \varphi_x^{(2)} = 1$ as in Figure 5, whereas for the anion $\varphi_x^{(1)} = \varphi_x^{(2)} = 2$. For clarity of comparison, the figure reports both profiles to evidence the different positions of their concentration peaks on the x axis.

x-scale of Figures 5–7 representative of the average mutual distance of the dislocations of Figure 2 with respect to the actual size of the electrolyte for ions 1 and 2 of Figure 4 respectively. Figure 5 shows bell-shaped x-profiles at any z/z_o; as expected, the peak values are well aligned at increasing z/z_o. The integral on x/x_o of each curve, proportional to the respective concentration of ion 1 at $y = 0$, agrees with the statistical trend sketched in Figure 4. Figure 6 confirms these results: the ion 2 is also described by bell-shaped profiles aligned along a straight direction through the electrolyte. These results substantiate therefore the previous considerations about Equation (39). It is remarkable the fact that the stress field of properly oriented dislocations provides a 'focusing' effect on the ions, whose explanation is

simple: whether the ions are channelled in the stretched zones or bounce between the extra-planes, it is reasonable to expect that the side components of their velocity are progressively damped by anelastic collisions with the atoms/ions of the surrounding lattice, e.g. converting into heat the kinetic energy loss, whereas the forward component is practically unaffected. The fact that the in-depth profiles of both ions overlap with good approximation justifies the concept of channelling, thanks to which the dislocations provide an efficient effect of directional focusing. Of course shape and position of the profiles are time dependent during the working life of the cell because of the functions defining c_i; yet further simulation tests indicate that the figures reported here, although obtained with a unique set of values of ξ, φ_x, φ_y, φ_z corresponding to one time only, are elucidative of the kind of information achievable through Equation (39). Hence, rather than reporting similar plots for further values of y, it seems more useful to highlight how the model accounts for the more complex dynamics of the ions in the presence of screw dislocations or, mostly important, in the stress fields of several dislocations. Let us generalize Equation (39) introducing the linear combination of an arbitrary number of functions $c_i^{(k)}$ having the form of Equation (31):

$$\begin{aligned} c_i &= \sum_k \alpha_k c_i^{(k)}, \\ c_i^{(k)} &= c_i^{(k)}\left(\varphi^{(k)}, \xi_i^{(k)}, \varphi_x^{(k)}, \varphi_y^{(k)}, \varphi_z^{(k)}\right), \\ (\varphi^{(k)})^2 &= (\varphi_x^{(k)})^2+(\varphi_y^{(k)})^2+(\varphi_z^{(k)})^2 \end{aligned} \tag{40}$$

The last condition ensures the validity of such a solution, whereas now $c_i^0 = \sum_k \alpha_k c_i^{0(k)}$ fulfil the boundary condition of initial concentration of the ith species. The arbitrary coefficients α_k and the time functions can be exploited in various ways: for instance, to combine the concentration profiles of Equation (31) into a unique 'flat' or 'top-hat' x-profile convolution of several bell-shaped profiles. In this case, however, the flat profile is not due to the unfavourable orientation of the dislocations, rather it is a cumulative feature of their particular arrangement; alternatively, indeed, it is also possible to obtain several bell curves spaced with each other so as to simulate as many ion confinement micro/nano-channels like that of Figures 5 and 6 expected with the array of several dislocations of Figure 3. So in a situation like that schematically depicted in this figure one reasonably expects that between two grains transits a 'grid' of micro/nano ion spots corresponding to the channels made available by the local arrangement of grain boundary dislocations; the grain size appears fundamental to fix the space scale of the ion grid. This focusing effect could be the basic feature of the so-called ion highways, as the reduction of lateral spread enhances the efficiency of charge transport between the electrodes; in other words, the previous considerations suggest that the high concentration ratio peak/ground of Figures 5 and 6 provides itself an indirect proof of the increased charge transport efficiency attainable via dislocation driven channelling. This chance is in fact realistic from an experimental point of view, as the dislocation structures of Figure 3 are indeed obtainable in practice with appropriate heat treatments of the solid oxide. In principle, the ion micro-beams coming out from one grain can or cannot match an analogous structure of favourably oriented dislocations in a neighbour grain; if not, the straightforward ion highway breaks off and the grain boundary resistivity increases. Either chance is easily quantified simply repeating the previous calculations in a grain boundary with choice of φ_x and φ_y with respect to ξ typical of favourably or unfavourably oriented dislocations with respect to the ion flow coming out from the former grain; after that, the respective values of $\sigma_{i,gb}^{\text{eff}}$ can be calculated with appropriate input values of $c_{i,gb}^0$ and $D_{i,gb}^0$ and then compared. The coefficients α_k add therefore further freedom degrees that account for the way any dislocation arrangement and orientation affect the ion transport. Of course, exactly as shown before, each mathematical strategy of simulation defines the corresponding z-profiles of concentration and eventually the total statistical distribution of each charge carrier in the electrolyte; this procedure finds its own outcome ending into the respective expressions of electric potential and power, Equations (30) and (38), to which each numerical test is correlated through the c_i themselves. A closing comment concerns the positions on the x-axis of the concentration peaks of Figures 5 and 6. With the given simulation parameters indicated in Figure 4, deliberately chosen equal for ions of both signs, the concentration peaks fall with good approximation on the same position of the x axis despite in general $x_1^{\max} \neq x_2^{\max}$; although the half maximum widths of the curves around the peaks are slightly different, it is possible to conclude that with the present choice statistically both ions share a similar path in the lattice. Typical ions for which this idea is intuitively reasonable are H^+ and $O^=$; as shown in Figure 2, the same two dislocations could channel the former in the stretched zone and the latter between the extra-planes because of stress field. In any case, the concentrations of ions sharing the same path through the most favourable crystal planes and vacancies are related to each other; with the mathematical choice of equal time functions defining both c_i, therefore, it is not surprising that the well-known condition $t_+ + t_- = 1$ holds. In addition, it is reasonable to think that in this case the ion conduction can occur in the same phase. Yet, if in general the set of time functions is different for the various ions, the concentration peaks correspond to different points of the x and y axes; i.e. the most probable ion paths along the z-axis of the electrolyte resulting from Equation (39) are different. An example

Int. J. Energy Res. 2011; **35**:1056–1074 © 2011 John Wiley & Sons, Ltd.
DOI: 10.1002/er

is reported in Figure 7 for the x axis only, which shows that the peaks of positive and negative ions can be effectively simulated to describe different paths in the lattice. With a different choice of all simulation parameters, however, the physical constraint $t_+ + t_- = 1$ does not necessarily hold longer as there is no direct mathematical link between c_i of the various ions: moreover, it is natural to justify the splitting of the most probable paths of anion and cation as a consequence of their motion in different phases, e.g. grain bulk and grain boundaries; thus the appropriate choice of x_o and the respective simulation parameters controlling the peak splitting, here arbitrarily chosen for mere clarification purposes, reflects in fact defined physical considerations, e.g. a grain size of specific interest. This figure evidences therefore the possibility of simulating even the more complex dislocation array of Figure 3 in a completely analogous way through the more flexible Equation (40) with trivial numerical methods of curve fitting. In conclusion, the present model recognizes and distinguishes important conduction mechanisms to be simulated and compared.

6. SUMMARY AND CONCLUSION

The paper emphasizes that, in addition to the etero/aliovalent doping, a key topic of the SOFC science is also the lattice defect structure of the solid oxides with which the charge carriers interact. The macro-scale model provides a systematic approach to describe how lattice defects and chemical composition of solid oxides affect the ion/multi-ion conductivity. No special hypothesis has been made on the nature or physical properties of the solid oxide, hence, the mathematical scheme introduced in section 3 holds in principle for any kind/grain size of solid oxide. Owing to the 3D mathematical formalism, the simplest case of a single crystal or large crystal core is straightforwardly extended to the more interesting and realistic case of a polycrystalline solid oxide with grain boundaries of desired width; geometrical considerations define the grain sizes as volumes of solid oxide around which are introduced layers with altered chemical composition and defect structure. In both cases the mathematical approach exploits two input data only that embody and summarize microstructural details, i.e. the diffusion coefficients of various charge carriers and their initial concentrations in the solid oxide. The model introduces also integration constants and time dependent functions to be regarded as input parameters of simulation: for instance the arbitrary function $\xi(t)$ introduced in Equation (31) controls the time profile of the cell power, in particular of the ramp up and ramp down transients, while the functions $\varphi_x(t)$, $\varphi_y(t)$, $\varphi_z(t)$ characterize the spread of ion paths through the electrolyte. The first equations (30) and (38) define then ϕ and W resulting as a function of these transport features. The input information can be provided by experimental measurements or calculated through separate micro-scale models. The latter chance is particularly valuable when the required information is difficult to be experimentally obtained. On the one hand, any approach '*ab initio*' is by itself a unique source of knowledge allowing to justify the altered values of the boundary layers and to quantify them; on the other hand, the limit on the number of atoms realistically tractable with reasonable computing times makes it difficult to extend the outcomes of atomistic models to the macro-scale. As the previous considerations emphasized that the grain boundary defect structure depends on the point and line defect dynamics along selected lattice planes, the global ion conductivity of practical interest is in fact a statistical property as a result of by many different grains randomly oriented with respect to the average direction of ion flow under the applied electric potential. Since just this kind of information is typically achievable through a macro-scale approach, the obvious conclusion is that linking together the outcomes of both theoretical models is the most rational and exhaustive route towards the design of advanced electrolytes and electrode/electrolyte interfaces.

REFERENCES

1. Maclagan RGAR. Ab initio calculations on [Pt–O–H] systems. *Journal of Molecular Structure* 2001; **536**:117–122.
2. Jacob T, Merinov BV, Goddard WA. Chemisorption of atomic oxygen on Pt(1 1 1) and Pt/Ni(1 1 1) surfaces. *Chemical Physics Letters* 2004; **385**: 374–377.
3. Stamenkovich VR, Fowler B, Mun BS, Wang G, Ross PN, Lucas CA, Markovic NM. Improved oxygen reduction activity on $Pt_3Ni(111)$ via Increased Surface Site Availability. *Science* 2007; **315**(5811):493–497.
4. Tanner CW, Fung KZ, Virkar AV. The effect of porous composite electrode structure on solid oxide fuel cell performance: part I—theoretical analysis. *Journal of Electrochemical Society* 1997; **144**(1): 21–30.
5. Huang RWJM, Chung F, Leeuw SW. Ion transport in nanocrystalline materials: a computer simulation study. *Journal of Electroanalytical Chemistry* 2005; **584**(1):44–53.
6. Reifsnider K, Huang X, Ju G, Solasi R. Multi-scale modeling approaches for functional nano-composite materials. *Journal of Materials Science* 2006; **41**: 6751–6759.

7. Pornprasertsuk R, Cheng J, Huang H, Prinz FB. Electrochemical impedance analysis of solid oxide fuel cell electrolyte using kinetic Monte Carlo technique. *Solid State Ionic* 2007; **178**:195–205.
8. Otsuka K, Kuwabara A, Nakamura A. Dislocation-enhanced ionic conductivity of yttria-stabilized zirconia. *Applied Physics Letters* 2003; **82**(6):877–879.
9. Lai W, Haile SM. Impedance spectroscopy as a tool for chemical and electrochemical analysis of mixed conductors: a case study of ceria. *Journal of the American Ceramic Society* 2005; **88**(11): 2979–2997.
10. Freeman SA, Booske JH, Cooper RF. Modeling and numerical simulations of microwave-induced ionic transport. *Journal of Applied Physics* 1998; **83**(11):5761–5772.
11. Fast JD, Van Bueren HG, Philibert J. *La Diffusion dans les Metaux*. Bibliotheque Technique PHILIPS: Eindhoven, 1975.
12. Zhu B. Solid oxide fuel cell (SOFC) technical challenges and solutions from nano-aspects. *International Journal of Energy Research* 2009; **33**: 1126–1137.
13. Cheng J, Prinz F. Damage in yttria-stabilized zirconia by Xe irradiation measured by X-ray diffraction. *Nuclear Instruments and Methods in Physics Research* 2005; **B227**:577–583.
14. Pornprasertsuk R, Ramanarayanan P, Musgrave CB, Prinz FB. Predicting ionic conductivity of solid oxide fuel cell electrolyte from first principles. *Journal of Applied Physics* 2005; **98**:103513-1–103513-8.
15. Kittel C. *Introduction to Solid State Physics*. Wiley: New York, 1967.
16. Honeycombe RWK. *The Plastic Deformation of Metals*. Edward Arnold Ed., Surrey, U.K., 1977.
17. Formby CL, Owen WS. Resistivity study of strain-ageing in Ta-o and Nb-o. *Acta Metallurgica* 1966; **14**(12):1841–1849.
18. Ogbuji LUJ. Plastic flow in the sintering of alumina. *Ceramics International* 1986; **12**:195–202.
19. Snow JD, Heuer AH. Slip systems in Al_2O_3. *Journal of the American Ceramic Society* 2006; **56**:153–157.
20. Carter CB, Norton MG. *Ceramic Materials*: *Science and Engineering*. Springer: New York, 2007; 315 ff.
21. Hong G-W, Lee J-Y. The interaction of hydrogen with dislocation in iron. *Acta Metallurgica* 1984; **32**(10):1581–1589.
22. Stephens DL, Alford WJ. Dislocation structures in single-crystal Al_2O_3. *Journal of the American Chemical Society* 1964; **47**:81–86.
23. Seo W-S, Koumoto K. Kinetics and mechanism of stacking fault annihilation and grain growth in porous ceramics of β-SiC. *Journal of Materials Research* 1993; **8**(7):1644–1650.